

# Application of Pharmacokinetic-Pharmacodynamic Modeling and Simulation for Antibody-Drug Conjugate Development

Aman P. Singh • Young G. Shin • Dhaval K. Shah

Received: 30 July 2014 / Accepted: 12 January 2015 / Published online: 11 February 2015  
© Springer Science+Business Media New York 2015

**ABSTRACT** Characterization and prediction of the pharmacokinetics (PK) and pharmacodynamics (PD) of Antibody-Drug Conjugates (ADCs) is challenging, since it requires simultaneous quantitative understanding about the PK-PD properties of three different molecular species *i.e.*, the monoclonal antibody, the drug, and the conjugate. Mathematical modeling and simulation provides an excellent tool to overcome these challenges, as it can simultaneously integrate the PK-PD of ADCs and their components in a quantitative manner. Additionally, the computational PK-PD models can also serve as a cornerstone for the model-based drug development and preclinical-to-clinical translation of ADCs. To provide an overview of this subject matter, this manuscript reviews the PK-PD models applicable to ADCs. Additionally, the usage of these models during different drug development stages (*i.e.*, discovery, preclinical development, and clinical development) is also emphasized. The importance of PK-PD modeling and simulation in making rationale go/no-go decisions throughout the drug development process is also highlighted. There is an array of PK-PD models available, ranging from the systems models specifically developed for ADCs to the empirical models applicable to all chemotherapeutic agents, which one can employ for ADCs. The decision about which model to choose depends on the questions to be answered, time at hand, and resources available.

**KEY WORDS** antibody-drug conjugate (ADC) · model based drug development · modeling and simulation · pharmacodynamics · pharmacokinetics · PK-PD · preclinical-to-clinical translation

## ABBREVIATIONS

ADC	Antibody-drug conjugates
ADME	Absorption, distribution, metabolism and elimination
AUC	Area under the curve
DAR	Drug: antibody ratio
ELISA	Enzyme-linked immunosorbent assay
IgG	Immunoglobulin G
IV	Intravenous
MIVC	<i>In vitro-in vivo</i> correlation
LC-MS	Liquid chromatography-mass spectrometry
mAb	Monoclonal antibody
MBDD	Model-based drug development
mPBPK	Minimal physiologically-based pharmacokinetic
MTD	Maximum tolerated dose
NCA	Non-compartmental analysis
ORR	Objective response rate
PBPK	Physiologically-based pharmacokinetic
PD	Pharmacodynamics
PFS	Progression free survival
PK	Pharmacokinetics
PK-PD	Pharmacokinetics-pharmacodynamics
PK-TD	Pharmacokinetics-toxicodynamics
PP	Proliferating population
TDC	ThioMab-drug conjugates
T-DM1	Trastuzumab-emtansine
TGI	Tumor growth inhibition
TI	Therapeutic index
TSC	Tumor static concentration
TV	Tumor volume

A. P. Singh • D. K. Shah (✉)  
Department of Pharmaceutical Sciences, School of Pharmacy and  
Pharmaceutical Sciences, The State University of New York at  
Buffalo, 455 Kapoor Hall, Buffalo, New York 14214-8033, USA  
e-mail: dshah4@buffalo.edu

Y. G. Shin  
College of Pharmacy, Chungnam National University, Daejeon, South  
Korea

## INTRODUCTION

Antibody-Drug Conjugates (ADCs) are immunoconjugates, consisting of one to several potent small molecule anticancer

drugs attached to monoclonal antibody (mAb) *via* chemical linker. The average number of drug molecules attached to the mAb is known as Drug: Antibody Ratio (DAR), which can dynamically change with time, making ADCs a heterogeneous modality. ADCs are one of the fastest growing class of anticancer agents with exceptional clinical efficacy (30–90% objective response rates with monotherapy) (1,2). They act *via* targeted delivery of the cytotoxic drugs to the cancer cells (3). Once administered in the body, the mAb helps target the ADC specifically to the tumor. Once outside the antigen expressing cancer cells, the ADC binds to the targeted antigen *via* mAb and internalizes. Upon internalization, the drug either leaves the mAb during the endolysosomal process, or gets liberated in the lysosome following digestion of the ADC. Once released, the drug diffuses within the cell and reaches the site of action (*e.g.*, microtubules, DNA), where it elicits the pharmacology (3).

Although the concept behind developing ADCs (*i.e.*, combining the specificity of mAb with the cytotoxicity of small molecule drugs) is simple and has been around for decades, the development of these molecules is very challenging (4). The main challenge comes from the need to simultaneously optimize and characterize three different entities of the conjugate (*i.e.*, the mAb, the drug, and the linker), which collectively determine the properties of an ADC (5). Correspondingly, characterization and prediction of the pharmacokinetics (PK) and pharmacodynamics (PD) of an ADC is also challenging, since it requires a simultaneous quantitative understanding about the PK-PD properties of the three different analytes *i.e.*, the mAb, the drug, and the conjugate. Mathematical modeling and simulation provides an excellent tool to overcome these challenges, as it can simultaneously integrate the PK-PD of ADCs and their components in a quantitative manner. Additionally, the computational PK-PD models can also serve as a cornerstone for the model-based drug development (MBDD) and preclinical-to-clinical translation of ADCs (6,7). Thus, PK-PD modeling and simulation is very useful to ADC discovery and development scientists in making rationale go/no-go decisions throughout the drug development process. To provide an overview of this subject matter, in this manuscript we have reviewed the PK-PD models that can be utilized for the development of ADCs. Additionally, we have emphasized the application of these models during different drug development stages *i.e.*, discovery, preclinical development, and clinical development.

## DISCOVERY

At the discovery stage the PK-PD modeling and simulation can be used to quantify selected parameters of interest for all the lead ADCs, which are then compared across the lead compounds to select the candidate ADC. These parameters, and hence the models used to quantify them, may pertain to PK or PD of the ADCs.

## PK Models

One of the most important properties for an ADC is the stability of the conjugate in the systemic circulation, which determines ADC PK *in vivo*. At the discovery stage, this stability is evaluated by incubating ADCs in plasma or buffer solution (8). Since the mAbs can also be unstable in these solutions, measuring total mAb or ADC (*i.e.*, conjugated mAb) concentrations alone does not provide the real idea about the stability of the ADC conjugate. Hence both (total mAb and ADC) concentration *vs.* time profiles are usually measured and fitted simultaneously using simple compartmental model like the one shown in Fig. 1a, to quantitatively characterize the stability of ADCs. In the model shown in Fig. 1a,  $k_{deg}$  represents the first order degradation rate of mAb in plasma/buffer, and  $k_{dis}$  helps characterize the decline in conjugated mAb concentrations that are usually measured using ELISA. It is important to note that in the absence of detail LC/MS data about the concentrations of each DAR species of an ADC, it is very difficult to estimate the true dissociation rate(s) of drug from ADC. Thus, the parameter  $k_{dis}$  serves as surrogate parameter that approximates the dissociation rate of drug from the ADC by characterizing the data in a phenomenological manner. When characterizing the concentration *vs.* time profiles of total mAb in plasma/buffer, only  $k_{deg}$  is active, whereas for characterizing ADC profiles  $k_{dis}$  is also active. Similar kind of PK models (as shown in Fig. 1b) can also be used to compare the stability of ADCs *in vivo*, as the *in vivo* dissociation rate of the drug from ADC can be estimated *via* simultaneous characterization of total mAb and ADC PK data. Figure 1b describes a 2-compartment model that has been used to characterize the PK of total mAb and ADC together (7,19), where the *in vivo* dissociation rate of the drug from ADC ( $k_{dis}$ ) is active only while characterizing the PK of ADC. It is also worth mentioning that the parameter  $k_{dis}$  can not only be used to compare *in vitro* or *in vivo* stability of different ADCs, but can also be used to establish an *in vitro-in vivo* correlation (IVIVC) for ADC stability.

Cellular level PK of different lead ADCs and its components in targeted cancer cells or other toxicity-prone tissues can also be compared at the discovery stage using mathematical modeling. Ideally a promising ADC would demonstrate only antigen mediate uptake in the cells, and would allow efficient release of the drug inside the cells, which should ideally demonstrate prolonged retention in the cell. A measurement of each of these processes involved in the cellular disposition of ADC and its components, and the quantitation of ADC and its component inside and outside the cells, is necessary to optimize the properties of all three components of an ADC (*i.e.*, the mAb, the linker, and the drug). However, since the direct measurement of all of these processes may not be feasible, they can be indirectly quantified by characterizing *in vitro* PK data for ADC and its components using cellular

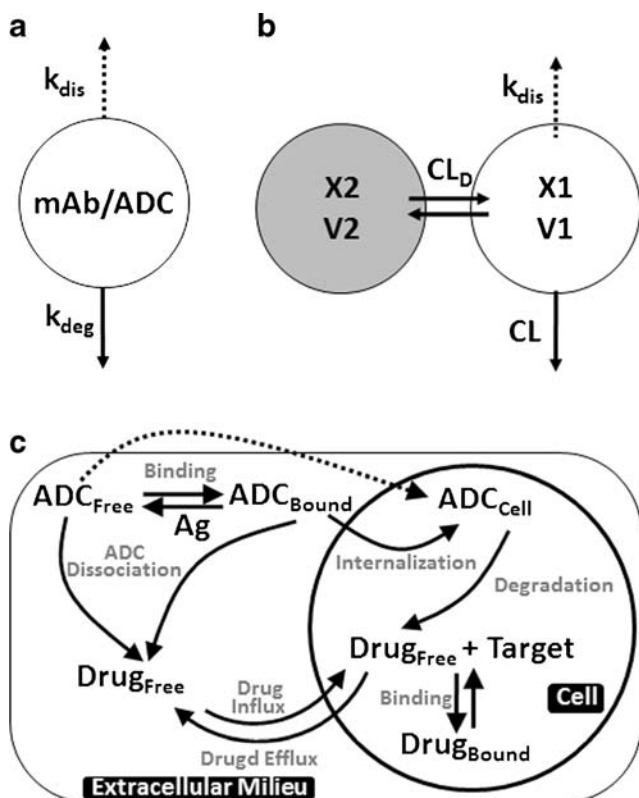


**Fig. 1** PK models for ADCs applicable at the discovery stage. **(a)** A 1-compartment model that can be used to simultaneously characterize the concentration vs. time profiles of mAb and ADC following incubation in plasma/buffer, to estimate the *in vitro* dissociation rate of the drug from ADC. **(b)** A 2-compartment model that can be used to simultaneously characterize the *in vivo* PK of mAb and ADC, to estimate the *in vivo* dissociation rate of the drug from ADC. **(c)** A cellular level systems PK model for ADCs that can be used to characterize or predict the PK of ADC and its components in cancer or other toxicity-prone tissue cells.

level PK models like the one shown in Fig. 1c (7). These models account for the binding of ADC/mAb to the cell surface antigen (Ag), internalization of the bound ADC/mAb in the cell, and degradation of the ADC/mAb inside the cell. These models also account for non-antigen mediated internalization (e.g., pinocytosis) of ADC/mAb in the cells (shown by dotted arrow in Fig. 1c). Along with the ADC and total mAb, the cellular level PK models also consider the disposition of unconjugated/released drug. Once the ADC is degraded inside the cell, the intact drug molecules are assumed to be released inside the cell, where either they can bind to the intracellular target (e.g., microtubules or DNA) or get effluxed out of cell *via* active or passive processes. These models also account for the dissociation of the drug from ADC outside the cells, and assume that any unconjugated drug outside the cells can be taken up by the cells using nonspecific processes (e.g., pinocytosis). Employing these models to quantitatively characterize the *in vitro* PK data for ADC and released drug in cells and media simultaneously, can help in estimating key parameters like the efflux rate of the released drug from the cells,

which is difficult to measure experimentally. Additionally, since the cellular level PK models are systems models, they can also be used for verifying experimentally obtained values of biomeasures (e.g., receptor number per cell, internalization rate of the antigen, intracellular target concentrations *etc.*), by comparing the quality of the *a priori* PK predictions made by the models using these biomeasures with the experimentally observed *in vitro* PK results (7,9).

## PD Models

In order to obtain an estimate of the efficacy for lead ADCs at the discovery stage, cell number *vs.* time profiles obtained following incubation of different ADC concentrations can be characterized using an *in vitro* PK-PD model, similar to the one shown in Fig. 2a. We believe that the efficacy estimates obtained using such PK-PD modeling based method are much more reliable than traditional point estimates like  $IC_{50}/IC_{90}$  values, since they consider the effect of ADC at more than one time point and also considers the dynamic nature of the system *e.g.*, the rate of tumor cell growth and kill. In the *in vitro* PK-PD model shown in Fig. 2a, the ADC concentrations in media ( $C_{in\ vitro}$ ) can either be assumed to stay constant or change with the time, according to the model shown in Fig. 1a. In Fig. 2a, the media ADC concentrations are assumed to induce cell killing in a concentration dependent manner, where the killing signal ( $k_{kill}$ ) is assumed to reach to the cells following a signal transduction delay ( $Tau_s$ ), and once the cells in the growth phase receive the signal, they are assumed to travel through a series of non-growing phases ( $Tau_c$ ) towards the death. The growth ( $k_g$ ) and kill ( $k_{kill}$ ) parameters obtained by fitting the model 2A to *in vitro* cell number *vs.* time data can be used to derive a matrix representing the efficacy of an ADC, which is termed as '*in vitro* tumor static concentration' ( $TSC_{in\ vitro}$ ) =  $\frac{k_g \cdot IC_{50, in\ vitro}}{k_{kill} - k_g}$  (10).  $TSC_{in\ vitro}$  is a theoretical concentration of ADC in the media that will impart steady-state levels of cell number in the culture media. This parameter represents the efficacy of an ADC for a given cell line, and can be used to compare different ADCs for triaging. Additionally,  $TSC_{in\ vitro}$  can be correlated with  $TSC_{in\ vivo}$  (described later in the manuscript) to establish an IVIVC for ADC efficacy. Of note, one can also derive a matrix similar to the  $TSC_{in\ vitro}$  to quantify *in vitro* toxicity of ADCs, which can then be used to triage ADCs based on their safety profile.

In order to identify a mechanistic biomarker and to achieve the proof-of-concept for the mechanism-of-action of ADCs, systems pharmacology models can also be employed at the ADC discovery stage. One of the simplest model of these kind is described in Fig. 2b, which can be used to characterize the effect of ADCs on different cell cycle phases (11). In particular, the model in Fig. 2b has been developed to characterize the changes in the population of cells belonging to different cell cycle phases, following the treatment with ADCs that can





It is important to quantify this instability of ADCs, not only to accurately characterize ADC PK, but also to predict the concentrations of unconjugated mAb and unconjugated drug, which may be responsible for reduced efficacy and enhanced toxicity of the ADC respectively. One simple way to characterize *in vivo* deconjugation of drug from ADC is by simultaneously fitting the *in vivo* PK data for total mAb and ADC (*i.e.*, mAb conjugated with at least one drug), obtained using ELISA A, by the PK model shown in Fig. 1b. This model provides the estimate for an average rate of drug dissociation from the ADC ( $k_{dis}$ ), which can also be used to calculate the average dissociation half-life of the drug *i.e.*, the time in which half of the drug molecules attached to the mAb will dissociate. However, as mentioned before, the estimates obtained using this method are only approximations.

Since the deconjugation process involves formation of the released drug by reduction of higher DAR species to lower DAR, accurate calculation of drug dissociation would ideally require measurement of DAR over time. This can either be done by measuring average DAR value of all the ADC molecules in the plasma, or by measuring the abundance of each individual DAR species, using sophisticated LC-MS/MS methods (14). The changes in average DAR values with time can be characterized using simple equations (*e.g.*, linear or exponential decline), which would yield the estimates for an aggregate rate or drug dissociation from ADC. However, accurate characterization of the changes in the proportion of each individual DAR species over time requires development of more sophisticated PK models. One such model has been developed by Bender *et al.* (Fig. 3a) to simultaneously characterize the disposition of different DAR species of trastuzumab emtansine (TDM-1), an ADC synthesized *via* random conjugation method (15). Total trastuzumab concentrations were measured by ELISA whereas each individual DAR species in the plasma sample were quantified by affinity-capture LC-MS technique. They used a catenary model to simultaneously characterize the dissociation of drug from each individual DAR species (DAR<sub>1</sub>-DAR<sub>7</sub>). When combined with a first order rate constant for the degradation of mAb in plasma ( $k_{plasma}$ ), the catenary model was able to well characterize the *in vitro* PK of total antibody and each DAR species of T-DM1 in rat and monkey plasma. When the catenary model and  $k_{plasma}$  was incorporated into the central compartment of a 3-compartment mammillary PK model with linear clearance ( $CL_{in vivo}$ ), the model was able to characterize *in vivo* PK of total antibody and each DAR species of T-DM1 in rat and monkey well. Since this model had an ability to analyze the dissociation of drug from each individual DAR species, the authors were able to identify that the rate of drug dissociation from high DAR species (*i.e.*,  $\geq 3$ ) was faster than lower DAR species. The estimated rate of DM1 dissociation from T-DM1 was similar for DAR<sub>7</sub> to DAR<sub>3</sub>, and this rate was 34–40% higher than the drug dissociation rate from DAR<sub>2</sub> ( $K_{2 \rightarrow 1}$ ). The dissociation rate of DM1 from DAR<sub>1</sub> ( $K_{1 \rightarrow 0}$ ) was the slowest, as it was

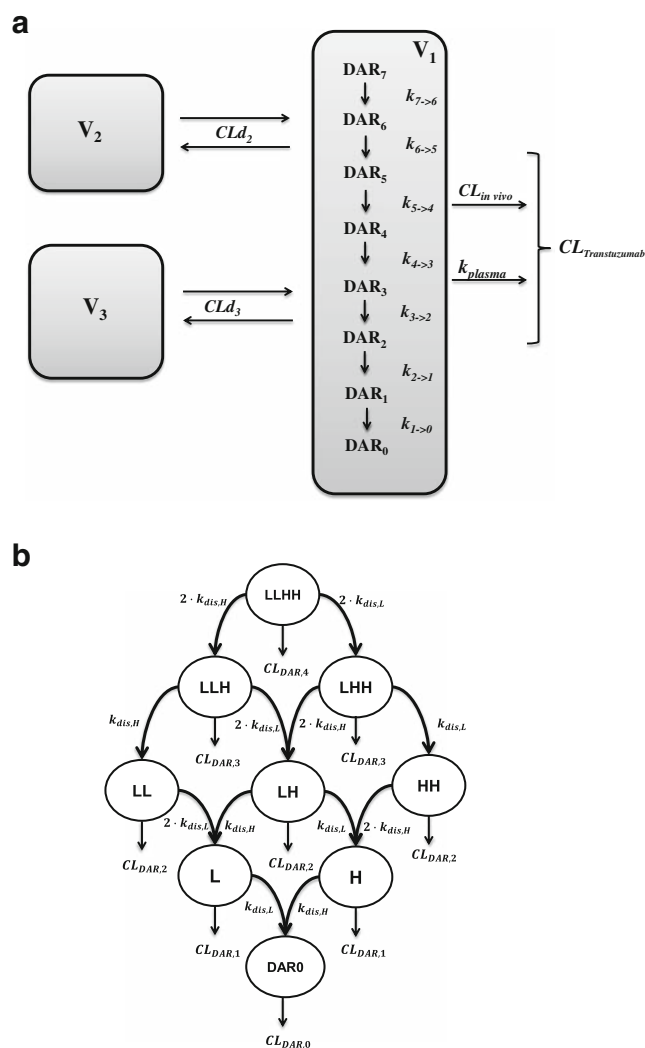


**Fig. 3** PK models developed to characterize the disposition of individual DAR species. **(a)** A PK model developed to simultaneously characterize the disposition of total trastuzumab and individual DAR species of trastuzumab emtansine (TDM-1), in rat and monkey (redrawn based on (15)). **(b)** A mechanism-based PK model developed for characterizing the differential clearance and drug deconjugation rates of individual DAR species of TH10MAB-drug conjugates (TDCs), in mice (redrawn based on (18)).

2.7–3.4 fold less than  $K_{2 \rightarrow 1}$ . Of note, for this model the authors assumed that each DAR species had the same elimination rate from the body, which may not be true for higher DAR species (16).

Since the ADCs like T-DM1 that are synthesized using random conjugation method have a broad distribution of DARs, and the location of drug attachment for the same DAR can also vary, there has been a great interest in synthesizing more homogenous ADCs using site-specific conjugation methods (17). The pattern of drug dissociation for these ADCs can be different and more amenable to quantitative characterization. Sukumaran *et al.* have proposed a PK model to characterize the dissociation of drug from the DAR species of one such ADC, known as ThioMab-drug conjugates

(TDC), in mice (Fig. 3b) (18). TDCs are made from mAbs with one engineered cysteine residue on each of the light (L) and heavy (H) chains, and can assume DARs of 0 to 4. In the Fig. 3b, DAR4 is shown as LLHH, DAR3 is shown as LLH or LHH, DAR2 is shown as LL or LH or HH, and DAR1 is shown as L or H. In order to accurately characterize the dissociation of drug from each DAR species ( $k_{dis}$ ), and to estimate the systemic clearance of each DAR species ( $CL_{DAR}$ ), the authors administered each purified DAR species in mice and measured the PK of all DAR species *in vivo*. Total mAb and TDC concentrations after administration of individual DAR species were measured using ELISA. The PK profiles of all DAR species in mice were characterized simultaneously using the model shown in Fig. 3b, where each DAR species was assumed to distribute according to a 2-compartment model (not shown in the figure). The model assumed that the rate of drug dissociation from each of the four sites of the TDC is different. It was assumed that one heavy chain and one light chain cysteine sites are more labile than the other two sites, and the rate of drug dissociation from more labile cysteines was assumed to be two times faster than the other two cysteines (*i.e.*,  $K_{dis,H} / K_{dis,L}$  vs.  $2 * K_{dis,H} / 2 * K_{dis,L}$ ). Additionally, the model also assumed that clearance of each TDC DAR species occurred from the central compartment and was proportional to the number of drug molecules attached. Thus, higher DAR species were assumed to eliminate faster than lower DAR species (*i.e.*,  $CL_{DAR,4} > CL_{DAR,3} > CL_{DAR,2} > CL_{DAR,1} > CL_{DAR,0}$ ). The proposed model was able to well characterize the complex deconjugation process of each DAR species for two different TDCs, and represents an important tool for the characterization and prediction of the *in vivo* stability and PK of other site-specific ADCs.

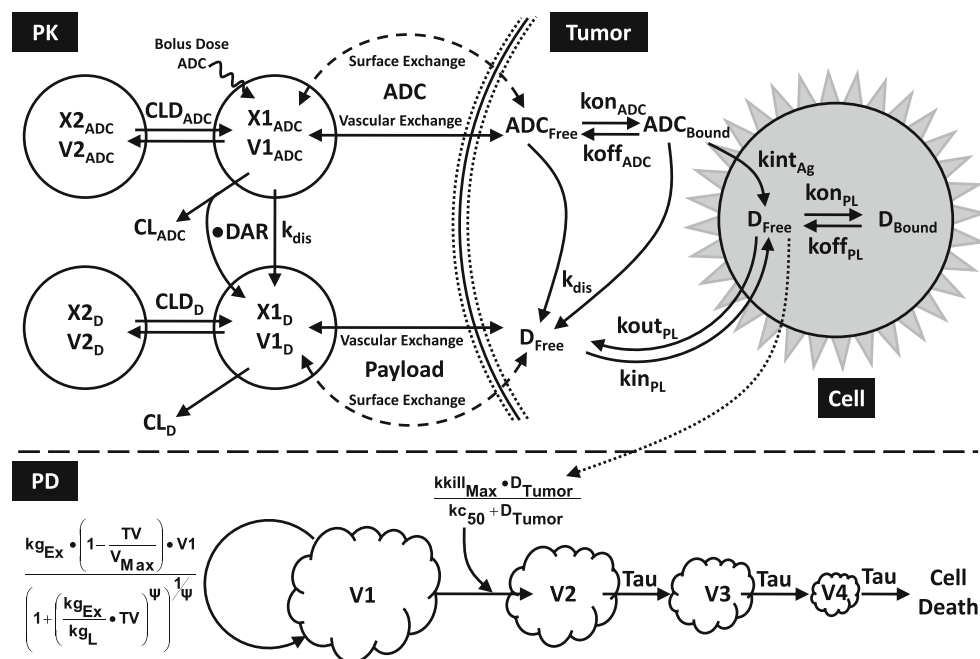
#### PK Model for Characterizing Tumor Concentrations of ADCs

While it is important to characterize and *a priori* predict the systemic PK of ADC and its components, characterizing and predicting the concentrations of these molecules at the site of action (*i.e.*, tumor) is equally important for establishing a reliable exposure-efficacy relationship. Since, in most cases tumor concentrations of small or large molecules are not in rapid equilibrium with the plasma concentrations, the relationships between plasma and tumor concentrations are established empirically. However, these empirical relationships are not reliable for extrapolation and *a priori* predictions. Thus, there is a need for more predictive PK models that can establish mechanistic relationships between plasma and tumor drug concentrations. One such model for simultaneously characterizing the PK of ADC and its components in plasma and solid tumor has been developed by us (Fig. 4) (7,19). The model characterizes systemic disposition of ADC using a 2-compartment PK model with linear clearance ( $CL_{ADC}$ ), and assumes that each molecule of ADC that is degraded will

generate drug molecules equivalent to the average DAR of the ADC at the time of clearance (changes in average DAR with time is characterized using monoexponential decline equation). The model also characterizes the systemic disposition of released drug using a 2-compartment PK model with linear clearance ( $CL_D$ ), and assumes that all the drug molecules generated following ADC degradation or nonspecific dissociation from the ADC ( $k_{dis}$ ) are entered into the central compartment of the model. Additionally, the model uses a systems PK component (20–23) to characterize the relationship between systemic and tumor concentrations of ADC and the drug. Since the tumors have higher interstitial pressure the model considers only diffusion mediated exchange of the molecules. The model assumes that when the tumor is small and avascular the main pathway of molecular exchange between the tumor and its surrounding is diffusion through the tumor periphery (surface exchange in Fig. 4), and when the tumor becomes bigger and vascularize the diffusion of molecules through blood vessels takes over (vascular exchange in Fig. 4). The parameters related to the exchange of ADC and drug molecules between blood and tumor (*i.e.*, diffusion, permeability *etc.*) are calculated based on their molecular weight and the size of the tumor. Once in the tumor microenvironment, the disposition of ADC and released drug is characterized using a cellular level systems PK model (similar to the one shown in Fig. 1c). Using two different ADCs, brentuximab-vedotin (SGN-35) and AlMcMMAF, we have shown that this multi-scale mechanistic model is capable of simultaneously characterizing the systemic PK of total mAb, ADC, and the released drug (7,19). Additionally, we have also demonstrated the ability of this model to *a priori* predict the tumor concentrations of total mAb, ADC, and the released drug, following systemic administration of two different ADCs in various xenograft bearing mice (7,19).

The tumor disposition model for ADCs is also a useful tool for better understanding the key parameters governing the plasma and tumor PK of ADC and its components, which can be valuable for designing better ADCs. For example, the sensitivity analysis of the model shown in Fig. 4 has suggested that the rate of drug dissociation from tumor and tumor size are two of the important parameters that can influence systemic exposure of the released drug (19). Along with these parameters, parameters like the efflux rate of the drug from cancer cells and the binding of drug inside the tumor cells were also found to be influential for drug exposure in the tumor (19). The model also suggested that the importance of systems parameters (*i.e.*, receptor number per cell, antigen internalization rate, and the affinity of mAb to cell surface antigen) in determining tumor drug exposure varies depending on the dose of the ADC (19). Pathway analysis of the ADC disposition model is also valuable in understanding the limitations of the system. For example, following the analysis of different pathways contributing to the systemic exposure of

**Fig. 4** A multi-scale mechanistic PK-PD model developed for ADCs. The model characterizes systemic and tumor PK of the ADC and the released drug. It uses tumor drug concentrations to drive ADC efficacy (redrawn based on (7)).



released drug following ADC administration, it was revealed that nonspecific degradation of ADC throughout the body contributes significantly to systemic drug exposure (19). Hence, the model suggested that no matter how tight is the linkage of the drug with mAb, one would always observe unconjugated drug concentrations in the systemic circulation following ADC administration. The ADC tumor disposition model can also be combined with PD models to establish clinically translatable PK-PD models (7) (Fig. 4), details of which are provided later in the manuscript.

#### PK Models to Characterize Whole Body Disposition of ADCs

Development of the exposure-toxicity relationships for clinically approved ADCs (T-DM1, SGN-35, and Mylotarg®) has been very challenging. There is no single analyte whose systemic exposure has been found to correlate very well with the toxicity of all the ADCs. One of the main reasons for this could be the limitation of the systemic compartment (*i.e.*, plasma/blood) in accurately representing the concentrations of different analytes at the site of tissue toxicity. Consequently, one may need to find out the concentrations of ADCs and their components in different tissues to establish an accurate and reliable relationship between ADC exposure and toxicity. However, in the clinical settings it is extremely difficult and sometimes not even possible to measure the concentrations of all these analytes across the whole body. Hence, mathematical models like the physiologically based PK (PBPK) models, which can be developed based on preclinical drug disposition data, provides an excellent alternative for characterizing and predicting the concentrations of ADCs and their components throughout the body.

The usage of PBPK models for the development of small molecules (24) and mAbs (25) is well recognized by now, and the development of these models is also becoming standardized. However, the PBPK models for ADCs are not yet established, and the development of these models entails unique challenges. One of the main challenges comes from the need to simultaneously account for the disposition of a large and small molecule (*i.e.*, conjugated mAb and unconjugated drug), whose ADME processes are governed by completely different physiological processes. For instance, one will have to account for the distribution of conjugated mAb (*i.e.*, ADC) in the whole body, metabolism of the conjugate all over the body, dissociation of the drug from the conjugate, distribution of the released drug in the body, and metabolism/elimination of the unconjugated drug, simultaneously. Thus, one would have to use both the small and large molecule PBPK models, and connect them in a mechanistic manner, in order to develop a PBPK model for ADCs. The proof-of-concept for the development of such a combined small and large molecule PBPK model has been recently demonstrated by us (26,27). We have combined the PBPK model of a small molecule anticancer drug topotecan (24) with the PBPK model for anti-topotecan mAb 8C2 (28), to *a priori* predict the effect of 8C2 on the plasma and tissue PK of topotecan. The model simultaneously accounted for the disposition of topotecan, 8C2, and the 8C2-topotecan complex (26).

We have employed a similar kind of combined PBPK model to simultaneously characterize the PK of ADC and the released drug. Our ADC PBPK model employs previously published platform PBPK model for mAb (25,29) to characterize the PK of ADC (*i.e.*, conjugated antibody), and uses a

separate small molecule PBPK model to characterize the PK of the released drug. Schematic of a representative tissue compartment of the ADC PBPK model is shown in Fig. 5a. It is assumed that the ADC will enter the tissue using arterial blood ( $Q$ ), and from the plasma compartment the ADC will either leave the tissue *via* venous blood ( $Q-L$ ), enter the endosomal space of vascular endothelial cells *via* pinocytosis ( $CL_{up}$ ), or will enter the tissue interstitial space *via* convection ( $L*(1-\sigma_v)$ ). Within the endosomal space the ADC will interact with FcRn and bound ADC will either recycle back to the plasma

compartment ( $FR$ ) or will reach to interstitial space *via* transcytosis ( $1-FR$ ). Each molecule of ADC that is degraded in the lysosome due to the lack of FcRn binding ( $k_{deg}$ ) is assumed to generate drug molecules equivalent to the DAR. Additionally, based on the linker properties, one can also assume that the drug may dissociate from the ADC during endosomal recycling. ADC molecules in the interstitial space are assumed to either leave the tissue *via* convection ( $L*(1-\sigma_i)$ ), enter back to vascular endothelial cells *via* pinocytosis, or interact with the targeted receptors (if present) on the tissue cells

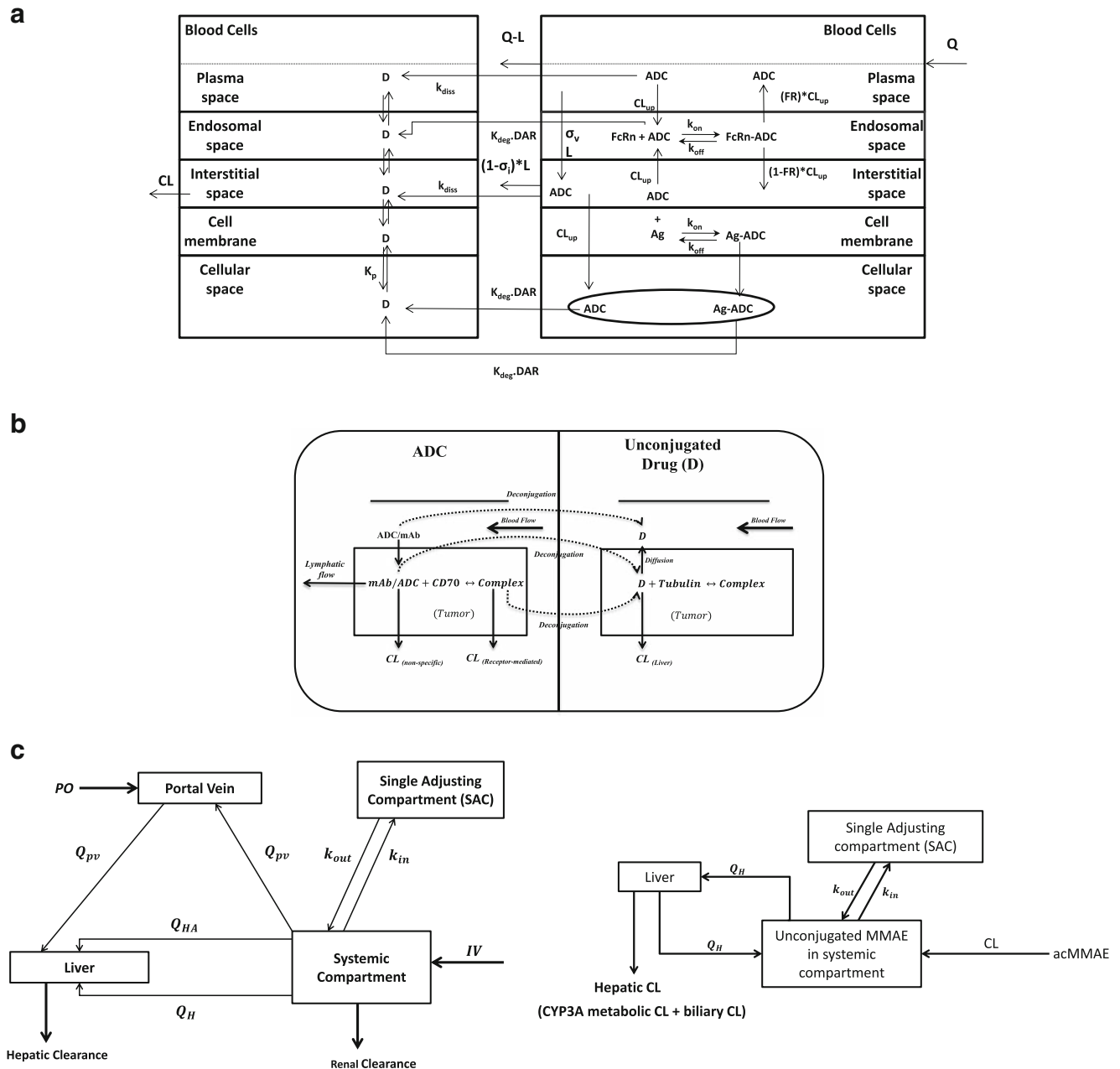


**Fig. 5** PBPK models for ADCs. **(a)** Schematic diagram of an ADC PBPK model, which combines the mAb PBPK model with the small molecule PBPK model in a mechanistic manner. **(b)** Tissue level diagram of a PBPK model developed to characterize the disposition of SGN-75 and cys-mcMMAF in tumor-bearing mice (redrawn based on (30)). **(c)** A minimal PBPK model developed for ADCs with MMAE as the conjugated drug (redrawn based on (31)).



(Ag). Within the target expressing cells, ADCs are assumed to internalize and degrade, while releasing the attached drug molecules (equivalent to DAR) back to the interstitial space. Additionally, based on the linker property, drug can also be assumed to dissociate from the ADC either in the plasma or interstitial space of a tissue ( $k_{dis}$ ). Once the drug ( $D$ ) is released in any of the tissue compartments, it will be assumed to rapidly distribute within the plasma, endosomal, and interstitial compartments. And, based on the drug's physicochemical properties, it will be assumed to distribute to the blood cells or tissue cells, and exhibit specific or nonspecific binding ( $K_p$ ). Unbound drug in the tissue will be assumed to leave the tissue *via* venous blood and will be allowed to enter other tissue compartments *via* arterial blood, following systemic distribution. Additionally, based on the drug's properties, unbound drug will be assumed to metabolize or eliminate unchanged in the relevant organs (e.g., kidney, liver, or bile) ( $CL$ ).

Zhao *et al.* have independently developed a similar PBPK model to simultaneously characterize the disposition of anti-CD70 ADC SGN-75 and its released drug cys-mcMMAF in the plasma, tissues, and tumor of a xenograft bearing mice (30). The diagram of a representative tissue compartment from their PBPK model is shown in Fig. 5b. They characterize the whole body PK of ADC using a mAb PBPK model (28). And, the whole body disposition of the released drug was characterized using a typical small molecule PBPK model, where the partition coefficients of the released drug between plasma and tissues was estimated, and the clearance of the drug, which was characterized from the liver, was also estimated. In order to accurately characterize the PK of the ADC and the released drug in the tumor, the authors had to account for the presence of CD70 receptors on the cancer cell surface and the interaction of ADC with these receptors. Additionally, the authors also had to consider binding of the drug with the intracellular target tubulin, to characterize the tumor PK of the released drug well. The authors stated that the PK of the ADC and the released drug in the tumor was highly dependent on their binding to the CD70 antigen and tubulin, respectively. Moreover, a time-dependent decrease in the abundance of tumor tubulin was also found to be necessary to describe the tumor PK of the released drug well. The final model was able to capture the PK of the ADC and the released drug well in the plasma and many of the tissues, including the tumor. The authors concluded that the PBPK model developed for SGN-75 in mice would be beneficial in predicting the human disposition of the ADC (30).

Application of minimal PBPK (mPBPK) model has also been applied recently to predict potential Drug-Drug Interactions (DDI) after administration of ADCs (31). Chen *et al.* have developed a Simcyp®-based minimal PBPK model for anti-CD22-vc-MMAE using Phase-I PK data. The developed final model (Fig. 5c) consisted of two sub models; i.e., a minimal PBPK model for antibody-conjugated MMAE (acMMAE)

and a minimal PBPK model for released MMAE from the ADC. The acMMAE component of the model included the systemic compartment (for IV dosing) and liver/portal vein compartment (for oral dosing). Blood flows to the systemic and liver/portal vein compartments were fixed to the physiological values. Single adjusting compartment (SAC) was also included representing peripheral tissue distribution to effectively capture the bi-exponential PK profile. The volume of distribution ( $V_{ss}$ ) and total clearance ( $CL$ ) were fixed based on the non-compartmental analysis (NCA) estimates and rate constants representing transfer of acMMAE to peripheral tissue were fitted. The total  $CL$  of acMMAE was used as an input into the unconjugated MMAE sub model. The unconjugated MMAE model had a similar structure with a systemic, liver and SAC compartment. A 'bottom up' approach was used while developing unconjugated MMAE sub-model. *In vitro* values of intrinsic clearance ( $CL_{int}$ ) were obtained from the human hepatocytes and were scaled up to the human metabolic clearance using a well-stirred model. *In vivo* bile-duct cannulated rat studies demonstrated that biliary clearance accounts for 50% of the total clearance in rats. Hence, while developing the final model, the total clearance was obtained from the sum of "in vitro estimated metabolic clearance" and "biliary clearance". The  $V_{ss}$  for MMAE was obtained from the mechanistic tissue composition equation by Rogers and Rowland (31). The final PBPK model was able to capture the clinical PK data of anti-CD22-vc-MMAE with reasonable precision. The model was also validated by predicting the exposure of released MMAE after administration of Brentuximab Vedotin (SGN-35) using PK data from several clinical trials. Ultimately, the model was used to predict the DDI data from clinical study done with concomitant administration of SGN-35 and the interacting drug (Rifampicin, Midazolam and Ketoconazole). It was observed in the trial that PK of acMMAE (conjugated drug) was not affected with concomitant medication, whereas the PK of released MMAE (a substrate of CYP3A) was affected with concomitant medication. The PBPK model was able to capture the changes in AUC and  $C_{max}$  after concomitant administration of the interacting drugs well (31).

## PD Models

### Models for Exposure-Efficacy Relationship

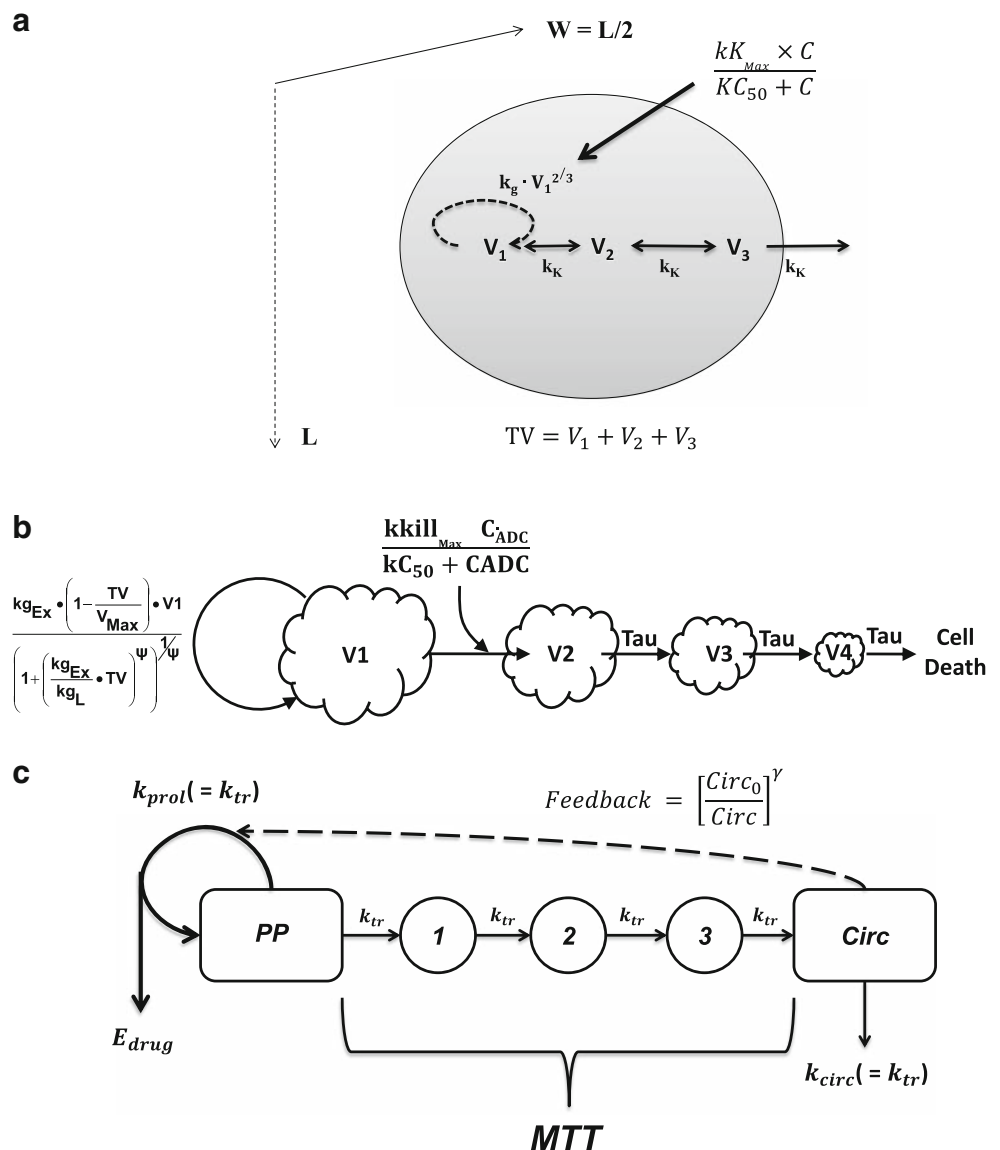
Establishing a clinically translatable PK-PD relationship based on the pharmacological data from animal models is very important at the preclinical development stage. Since most of the ADCs to date have been developed for oncology indications, development of these relationships usually involves tumor growth inhibition (TGI) data obtained following ADC administration in various xenograft bearing mice. The PD models employed to characterize ADC induced TGI data

are mostly developed based on the cell-distribution model (32) and the signal-distribution model (33), which are widely used generic PD models applicable to most anticancer drugs.

The first preclinical PK-PD model to characterize ADC induced TGI data was presented by Jumbe *et al.* (34). They employed the model to characterize the efficacy of T-DM1 in trastuzumab resistant mouse xenograft models following dose-ranging and dose-fractionation studies. The schematic of the PD model used by Jumbe *et al.* is provided in Fig. 6a. The authors characterized the systemic PK of ADC using a 2-compartment mammillary PK model with linear clearance, and used the central compartment ADC concentrations to drive the efficacy. A unique set of equations were used to characterize the growth of the tumor in the mice, where instead of directly multiplying the tumor volume with the expo-

nential growth rate ( $k_g$ ), volume raised to the power of 2/3 was used (please see (34) for explanation). The authors assumed that the ADC concentrations in the central compartment ( $C$ ) would induce its effect in a nonlinear manner, which was characterized using Michaelis-Menten type equation. In the Fig. 6a,  $kK_{MAX}$  is the maximum rate of drug effect and  $kC_{50}$  is the central compartment ADC concentration that will induce half of the maximal effect. Consistent with the cell-distribution model, the authors assumed that once the tumor cells are exposed to the ADC they shuttle from the growing compartment to a series of non-growing compartments at the rate of  $k_K$ , eventually leading to their death. The authors were able to use the model to simultaneously characterize the TGI data obtained following administration of different doses of T-DM1 in two different xenograft mouse models. In addition,

**Fig. 6** PK-PD models for ADCs applicable at the preclinical stage **(a)** A preclinical PK-PD model developed to characterize the efficacy of T-DM1 in trastuzumab resistant xenograft mouse models (redrawn based on (34)). **(b)** A semi-mechanistic PK-PD model developed to characterize the efficacy of AlimMMAF and T-DM1 in preclinical animal models (redrawn based on (10)). **(c)** A semi-mechanistic PK-PD model, which was originally developed to characterize chemotherapy-induced myelosuppression (redrawn based on (35)).



the authors introduced the concept of a secondary parameter known as tumor static concentration ( $TSC_{Jumbe}$ ), which they termed as a plasma ADC concentrations at which “tumor growth and death rates are instantaneously equal and tumor volume remains unchanged”  $TSC_{Jumbe} = \frac{K_g \cdot KC_{50}}{kK \cdot kK_{MAX} - K_g}$ . The TSC is a valuable parameter, since it represents the growth properties of a system as well as the efficacy and potency of the ADC. Jumbe *et al.* used this secondary parameter to guide the selection of clinical dosing regimen for T-DM1, where they recommended that the trough concentrations of the ADC between the two dosing intervals should not fall below the TSC, in order to achieve the antitumor activity (34).

Due to a few limitations of above described PD model (*e.g.*, numerical instability of the model, inflexibility of the growth function *etc.*), we have developed alternative PD model to characterize the efficacy of ADCs, by adapting the cell-distribution model (10). The model uses a 2-compartment linear PK model to characterize the systemic PK of the ADC, and the central compartment ADC concentrations are used to drive the PD model. Schematic diagram of the PD model is shown in the Fig. 6b. The model assumes that the tumor growth rate changes according to the tumor volume, where the tumor grows exponentially ( $kg_{Ex}$ ) when it is small, followed by a switch to the linear growth ( $kg_L$ ), and finally the tumor growth becomes negligible when the tumor volume ( $TV$ ) approaches the tumor carrying capacity of the body ( $V_{Max}$ ). The model assumes nonlinear killing by the ADC, which is governed by the maximum rate of killing ( $kkill_{Max}$ ) and the ADC concentrations that produces half of the maximum killing ( $kc_{50}$ ). The model assumes that once the tumor cells are exposed to the ADC, they travel from the growing compartment ( $V_1$ ) to a series of non-growing compartments ( $V_2$ – $V_4$ ) with the residence time of  $Tau$  in each compartment, eventually leading to their death. The model was able to characterize TGI data obtained following administration of two different ADCs (T-DM1 and A1mcMMAF) in multiple xenograft models reasonably well. A new derivation for the TSC value based on the improved PD model ( $TSC_{in vivo}$ ) was obtained:

$$\left( TSC_{in vivo} = \frac{kg_{Ex} \cdot kc_{50} \left( 1 - \frac{V_0}{V_{Max}} \right)}{kkill_{Max} \left( 1 + \left( \frac{kg_{Ex} V_0}{kg_L} \right)^{1/ - kg_{Ex} \left( 1 - \frac{V_0}{V_{Max}} \right)} \right)} \right), \text{ where } V_0$$

is the initial tumor volume. The  $TSC_{in vivo}$  was established as an efficacy index and it was used to guide preclinical-to-clinical translation of ADCs. It was hypothesized that in the clinic one would need to employ a dosing regimen that can at least achieve an average ADC exposure equivalent to the preclinically obtained  $TSC_{in vivo}$ , in order to attain the efficacy (*i.e.*, at least stable disease). The translational value of the  $TSC_{in vivo}$  was validated using T-DM1, where it was shown that the predicted range of the clinically efficacious dosing regimens for T-DM1 based on  $TSC_{in vivo}$  was very similar to

the clinically approved dosing regimen of 3.6 mg/kg Q3W (every 3 week) (10).

In both the PD models presented above, the plasma concentrations of ADCs obtained *via* ELISA, which quantifies concentrations of mAb conjugated to at least one drug molecule, were used to drive the efficacy. Since these PK-PD models do not directly consider changes in the DAR over time and differential potency of different DARs, a difference in the ADC stability between mice and human may make the pre-clinical PK-PD relationships developed using these models inferior for the clinic. Sukumaran *et al.* (18) have proposed an alternate method to remediate this issue, where they used the plasma PK of each individual DAR species to drive the ADC efficacy differently. They assumed that the killing rate of an ADC increases with DAR, and accordingly higher DAR species were assumed to kill the tumor faster than lower DAR species. Using simple exponential growth and nonlinear killing function driven by individual DARs, they were able to characterize the TGI data for two different TDCs in xenograft models satisfactorily. Thus, this model provides a better alternative for developing preclinical PK-PD models when individual DAR PK is available.

Since the properties of clinical tumors (*e.g.*, tumor size, antigen expression, efflux transporters *etc.*) can be significantly different than the tumors from animal models, the same plasma ADC concentration can lead to different drug exposure in preclinical *vs.* clinical tumors. Thus, preclinical PK-PD relationships developed based on the plasma concentrations may be suboptimal for preclinical-to-clinical translation of ADC efficacy. To overcome this challenge, one needs to develop a PK model that can establish a mechanistic link between the plasma ADC concentrations and tumor drug concentrations, and use the tumor drug concentrations obtained using such PK model to drive the PD model. We have developed one such systems PK model for ADCs, which can characterize and predict the tumor concentrations of ADC and the released drug following systemic administration of ADCs in preclinical animal models and cancer patients (7,19). Schematic diagram of the PK-PD model developed based on this systems PK model is shown in Fig. 4. This model uses intra-tumor concentrations of the released drug ( $D_{Tumor}$ ), instead of the plasma ADC concentrations, to drive the efficacy. Thus, it is capable of accounting for a different tumor exposure and hence different efficacy of an ADC in the clinic *cf.* preclinical models, at the same plasma PK of an ADC. An ability of this PK-PD model to facilitate the preclinical-to-clinical translation of ADC efficacy has been demonstrated using SGN-35. The developed model was first used to estimate the efficacy parameters for the ADC preclinically, by establishing a PK-PD relationship between the tumor drug concentrations and TGI data obtained from different xenografts. Subsequently, the systems parameters for preclinical tumors (*e.g.*, tumor growth

rate, tumor size, antigen expression level *etc.*) were replaced by the parameters obtained from the clinical tumors. The plasma PK of the ADC in mice was replaced by the human PK and, the DAR *vs.* time profile of the ADC in human was assumed to be the same as the monkey profile. Finally, the PK-PD model was used to simulate clinical trials, assuming the same efficacy of the released drug in preclinical and clinical tumors. The model was able to *a priori* predict the progression free survival (PFS) rates and objective response rates (ORR) for two different dosing regimens of SGN-35 in the cancer patients very well (7). Thus, in order to build clinically translatable PK-PD relationships for ADCs at the preclinical stage, it is advisable to employ more mechanistic PK and PD models like the one shown in Fig. 4 to characterize the preclinical data.

### Models for Exposure-Toxicity Relationship

Since a clinically viable ADC does not have to be the most potent one, but the one with the highest possible TI, understanding preclinical exposure-toxicity relationship for an ADC is also very important. However, due to the categorical and subjective nature of many ADC related toxicity indices (*e.g.*, peripheral neuropathy), it becomes difficult to establish a continuous PK-PD relationship for ADC toxicities (which is more appropriately referred to as PK-toxicodynamic (TD) relationship). Nonetheless, ADC induced toxicities affecting the blood cells (*e.g.*, thrombocytopenia and neutropenia) can be measured in a continuous manner, hence they are amicable to PK-PD modeling. Consequently, the semi-mechanistic PK-PD model developed by Friberg *et al.*, which is widely used to characterize the chemotherapy-induced myelosuppression (Fig. 6c) (35), can be applied to characterize exposure-toxicity relationships for ADCs. This model includes proliferating cell population (PP) (*e.g.*, stem cells and progenitor cells) as one compartment on which the drug acts ( $E_{drug}$ ), and measured circulating blood cells (*Circ*) as another compartment. The proliferating cells and observed cell populations are connected *via* three different maturing cells populations, characterized as transit compartments with the transit rate of  $k_{tr}$ . The model also assumes that the generation of new cells ( $k_{prol}$ ) is dependent on the number of circulating cells, and a feedback mechanism from the circulating cells is included. Tatipalli *et al.* have employed this model to characterize the neutropenia induced by 10 different ADCs in cynomolgus monkeys (36). All the 10 ADCs had the same drug-linker (vc-MMAE) and similar mAb scaffold (IgG), but different mAb target. A sequential approach for the PK-PD modeling was used, where first the PK of all 10 ADCs was characterized using a 2-compartment model with linear clearance. The toxicity of all ADCs were then characterized using the models shown in Fig. 6c, with the assumption that the toxicity of the ADCs is directly proportional to their plasma concentrations ( $E_{drug} = ADC_{plasma} * slope$ ), with '*slope*' as the efficacy parameter. The model was able to capture the toxicity of all the ADCs in the monkey

reasonably well, and despite having the same drug-linker the *slope* estimates for all the ADCs ranged about 10 fold. The authors stated that the model can be used for preclinical-to-clinical translation of ADC toxicity, and they believe that the clinical exposure-toxicity relationships for ADCs can be predicted based on the monkey toxicity data.

## CLINICAL DEVELOPMENT

During Phase-I the main focus is on determining the maximum tolerated dose (MTD) and optimal dosing regimen of the ADCs in relevant patient population. Whereas during Phase-II and III the focus is on developing a reliable exposure-response relationship for the ADC in the diverse patient population. Since the PK and PD data available from each subject in the clinic is much sparse than preclinical data, and there is a significant amount of inter-individual variability in the data, the PK-PD model development strategy at the clinical stage is different than the preclinical stage. Apart from estimating the model parameters, at the clinical stage a significant emphasis is also given on accurately estimating the inter-individual variability in these parameters, and identifying clinically significant covariates that can explain the inter-individual variability in the parameters. Thus, the structural PK-PD models used at the clinical stage are much simpler and less mechanistic than the preclinical stage models. However, the statistical component of the models, which is used to adequately characterize the population variability and identify covariates, is significant.

### PK Models

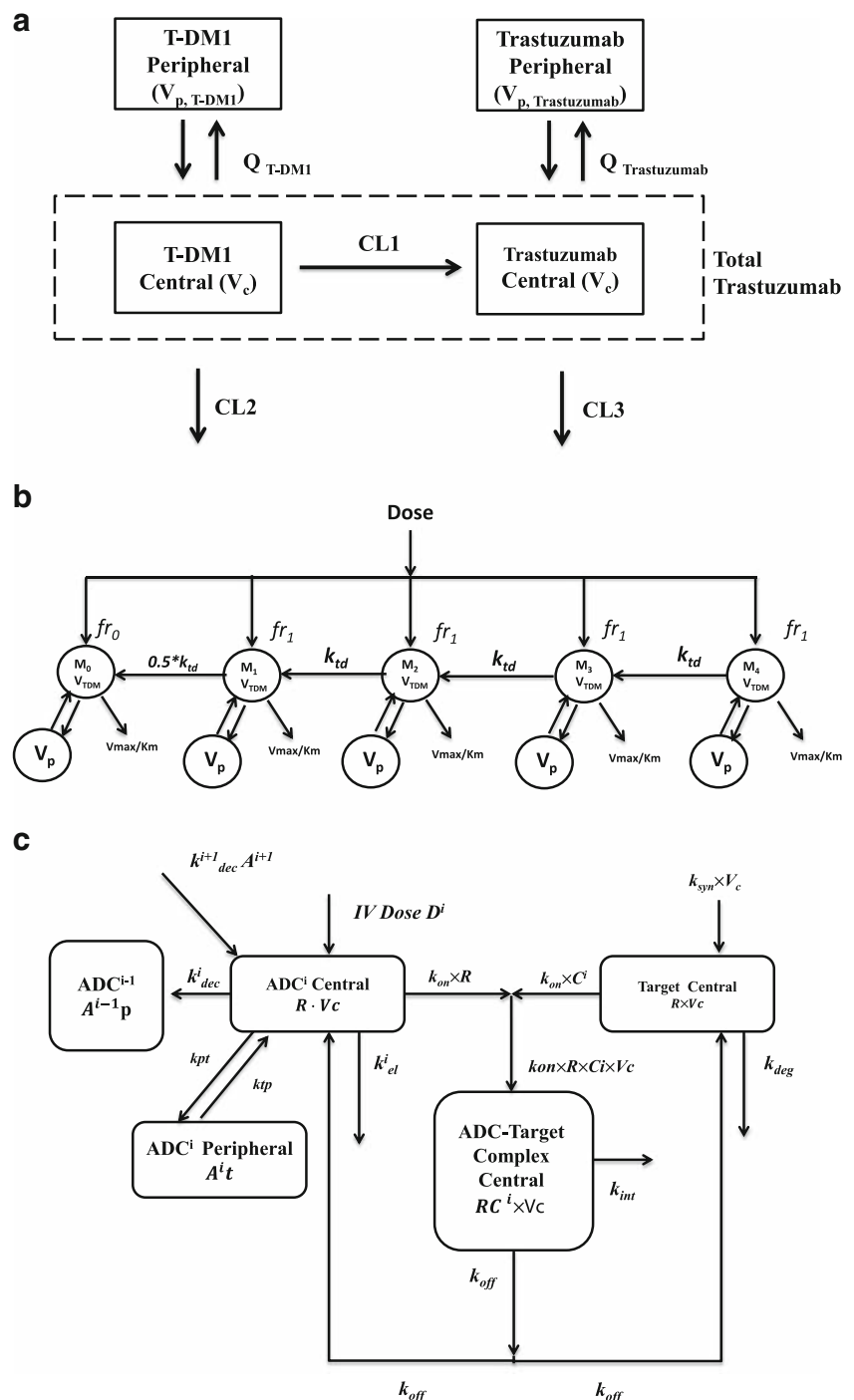
Most of the clinical PK models for ADCs have been developed based on T-DM1 clinical data. Depending on the number of analytes one wish to characterize with the PK model, the complexity of the model varies. One of the first and simplest model to characterize T-DM1 clinical PK has been developed by Gupta *et al.* (37) who used a 2-compartment model with linear elimination to simultaneously fit ADC (*i.e.*, conjugated mAb) PK data obtained from three different clinical studies. The authors were able to characterize the clinical PK of T-DM1 well. They were also able to estimate the inter-individual variability in PK parameters and significance of different covariates with good precision. The authors found that body weight, albumin, tumor burden, and aspartate aminotransferase levels were statistically significant covariates. However, only body weight was found to have a clinically meaningful effect on the inter-individual variability in PK parameters (*i.e.*, clearance and volume of distribution), and the rest of the covariates did not seem to affect the clinical PK of T-DM1. As a result, authors were able to conclude that no

further dose adjustment for T-DM1 was necessary in heavily pretreated patients with metastatic breast cancer. The same 2-compartment linear model was later demonstrated to be sufficient for characterizing T-DM1 clinical PK data obtained from much larger cohort of patients (38).

In order to simultaneously characterize the clinical PK of ADC and total antibody (*i.e.*, trastuzumab), Lu *et al.* have developed a PK model by combining two different linear 2-compartment models in a mechanistic manner (Fig. 7a) (39).

Plasma samples were analyzed for total trastuzumab and TDM-1 using two different ELISA methods. The authors assume that any molecule of trastuzumab that is conjugated with at least one molecule of DM1 (*i.e.*, the ADC) would have a different PK properties than the unconjugated trastuzumab. While the T-DM1 and trastuzumab were assumed to have the same central compartment volume of distribution ( $V_c$ ), their systemic clearance ( $CL2$  *vs.*  $CL3$ ), inter compartmental distribution clearance ( $Q_{T-DM1}$  *vs.*  $Q_{Trastuzumab}$ ), and volume of

**Fig. 7** PK models for ADCs applicable at the clinical Stage. **(a)** A PK model developed by combining two different linear 2-compartment models in mechanistic manner, to simultaneously characterize the clinical PK of T-DM1 and total trastuzumab (redrawn based on (39)). **(b)** A semi-mechanistic population PK model developed to simultaneously characterize T-DM1 and total trastuzumab clinical PK data (redrawn based on (40)). **(c)** A generic TMDD model developed for ADCs (redrawn based on (42)).





distribution for the peripheral compartment ( $V_{p,T-DM1}$  vs.  $V_{p,Trastuzumab}$ ) were assumed to be different. The model also assumed that the drug (DM1) dissociates from the ADC at the clearance rate of  $CL1$ , resulting in the formation of unconjugated mAb. The model was able to simultaneously characterize the PK of T-DM1 and total trastuzumab (i.e., T-DM1 + trastuzumab) obtained from several clinical studies reasonably well. The models also provided an insight into the relative clearances of ADC and mAb, where it was estimated that the clearance of T-DM1 conjugate is approximately 2–3 times faster than its parent antibody trastuzumab (39). The authors also used the PK model to optimize the sampling scheme for the measurements of T-DM1 and trastuzumab in the clinic. They recommended that since the model is able to accurately predict total trastuzumab PK based on the T-DM1 PK, only 3 PK samples for total trastuzumab (sampled at pre-infusion, end of infusion in cycle 1, and at the steady state cycle) should be sufficient for characterizing the entire PK profile with similar predictive accuracy to that of a dense PK sampling scheme (39).

Chudasama *et al.* have developed a more mechanistic population PK model to simultaneously characterize T-DM1 and total trastuzumab clinical PK data (Fig. 7b) (40). This model was developed by simplifying a model developed for characterizing the PK of different DAR species of T-DM1 in monkeys (Fig. 3a) (15). The unconjugated mAb ( $M_0$ ) was characterized using a 2-compartment model with nonlinear elimination ( $V_{max}/K_m$ ). And, the conjugated mAb (i.e., ADC) was assumed to be divided into 4 different DAR species ( $M1$ – $M4$ ), each of which was characterized using a 2-compartment model with nonlinear elimination. All the PK parameters (i.e.,  $V_{T-DM1}$ ,  $V_p$ ,  $CLD$ ,  $V_{max}$ ,  $K_m$ ) for the unconjugated mAb and each ADC DAR species were assumed to be the same. A first-order rate constant ( $k_{id}$ ) was used to characterize the dissociation of DM1 from M4, M3, and M2, whereas the dissociation of DM1 from M1 was characterized using half the value of  $k_{id}$  ( $0.5 \cdot k_{id}$ ). The fraction of dose administered as unconjugated mAb was characterized as  $fr_0$ , and the fraction of dose administered as the ADC was entered into each of the four compartment as  $fr_1$  (i.e.,  $1 - fr_0/4$ ). The model was able to characterize T-DM1 and total trastuzumab clinical PK data obtained following administration of a wide range of doses (0.3–4.8 mg/kg) at two different dosing regimen (Q3W and QW) reasonably well, including the target mediated elimination component conspicuous at the low doses (40). As such, the model provides a semi-mechanistic platform for understanding and characterizing the clinical PK of ADCs.

Since most of the ADCs are developed against rapidly internalizing and highly expressed tumor cell surface antigens, chances of observing the target mediated drug disposition (TMDD) (41) of ADCs in the clinic are high. To better characterize this type of PK, Gibiansky *et al.* have developed a generic TMDD model for ADCs (Fig. 7c) and its approximations (i.e., quasi-equilibrium (QE), quasi-steady-state (QSS) and michaelis-menten (MM)), using T-DM1 clinical PK data (42). In the generic model shown in Fig. 7c, each DAR species

of the ADC ( $ADC^i$ ) is assumed to follow a 2-compartment model with the same distribution characteristics ( $V_c$ ,  $k_{pt}$ ,  $k_{tp}$ ), and individualized first order elimination rates ( $kel^i$ ) that are assumed to be proportional to the number of drug molecules attached to the mAb (i.e., higher DAR=faster elimination). The model also includes binding ( $k_{on}$ ) and dissociation ( $k_{off}$ ) of each DAR species to the target receptor ( $R$ ) in the central compartment, and internalization ( $k_{int}$ ) of receptor bound ADC. Natural turnover of the target is also included using the zero order synthesis rate ( $k_{syn}$ ) and first order degradation rate ( $k_{deg}$ ). Deconjugation of drug from each DAR species is included in the central compartment using the first order deconjugation rate constant ( $k_{dec}^i$ ), which is assumed to be proportional to the DAR (i.e., higher DAR=faster drug deconjugation). Each DAR species are assumed to be generated from higher DAR species ( $ADC^{i+1}$ ) following drug deconjugation ( $k_{dec}^{i+1}$ ), and are also assumed to be eliminated to lower DAR species ( $ADC^{i-1}$ ) following drug deconjugation ( $k_{dec}^i$ ). The authors have simplified the generic TMDD model using different approximations (i.e., QE, QSS, and MM), to obtain models that can provide better identifiability and precision on the estimation of the parameters when only limited amount of data is available. The authors have also provided further simplification of the model by assuming that all DAR species have similar elimination rates ( $kel^i$ ) and deconjugation rates ( $k_{dec}^i$ ), which were assumed to be proportional to DAR in the generic model. It is important to note that the authors drew an analogy between their MM approximations and the nonlinear elimination pathway employed by Chudasama *et al.* (Fig. 7b) (40), and pointed out that in order to characterize the nonlinear elimination of each DAR species they have used total mAb concentration in the denominator with  $K_m$  instead of the concentration of each DAR species used by Chudasama *et al.*, which the authors believe is mechanistically more appropriate. The model by Gibiansky *et al.* was able to characterize the clinical PK data for TDM-1, simulated using the models developed by both Lu *et al.* (Fig. 7a) (39) and Chudasama *et al.* (Fig. 7b) (40), reasonably well (42). However, since the model was applied to very rich simulated datasets with considerably small inter-individual variability, application of the model to more realistic and sparse clinical data remains to be seen. Nonetheless, this PK model is flexible, mechanistic, and broadly applicable to other ADCs. And, the model also has the capability to fit the PK of individual DAR species, if available.

## PD Models

### Models for Exposure-Efficacy Relationship

Since the continuous measurement of tumor burden following ADC treatment is much difficult in patients *cf.* preclinical animal models, the number of published examples

characterizing ADC efficacy using a PK-PD model is scarce. Luu *et al.* have presented one such population PK-PD model to establish clinical exposure-response relationship for anti-CD22 ADC inotuzumab ozogamicin (CMC-544), in patients with refractory or relapsed indolent B-cell non-Hodgkin's lymphomas (43). They correlated the plasma PK of total drug (*i.e.*, conjugated + unconjugated calicheamicin) in each patient with their tumor size, which was determined from the sum of the products of tumor diameters. The tumor size data included measurements from the pre-screen time, during ADC treatment, and up to 15 months following the treatment. The PK of total drug ( $C_p$ ) was characterized using a linear 2-compartment model. The net tumor growth was characterized using a simple exponential growth equation ( $k_g$ ). And, the drug effect was characterized using a direct inhibitory effect ( $E$ ) on the tumor growth rate. Thus, the change in tumor size ( $T$ ) with time was characterized using the following equation:  $k_g \cdot (1 - E \cdot C_p) \cdot T$ . The model was able to characterize the tumor shrinkage and rebound for all the patients reasonably well. Simulations performed using the final model revealed that following the treatment with CMC-544 (given at 1.8 mg/m<sup>2</sup> every 28 days for a total of 4 cycles), median 10% tumor shrinkage can be seen around 35 days, with the peak shrinkage occurring around 161 days. The PK-PD model also revealed that following CMC-544 treatment the duration of response could be sustained beyond 1 year post treatment, and the tumor size may not return to the baseline for up to 2 years post treatment (43). Thus, the PK-PD model provided an improved understanding about the quantitative relationship between the time course of tumor response and CMC-544 treatment. Additionally, the model can also be used to further optimize the dose and dosing regimen of the ADC for future studies.

One can also employ more complex and mechanistic PK-PD models to characterize clinical tumor size *vs.* time profiles. For example, the PD model developed for *a priori* predicting the clinical efficacy of SGN-35 (Fig. 4) simulated tumor volume *vs.* time profiles for different patients (7). Thus, theoretically it can also be used to characterize the clinical tumor volume *vs.* time profiles. However, implementation of such models to characterize the efficacy data of ADCs at the clinical stage remains to be seen.

### Models for Exposure-Toxicity Relationship

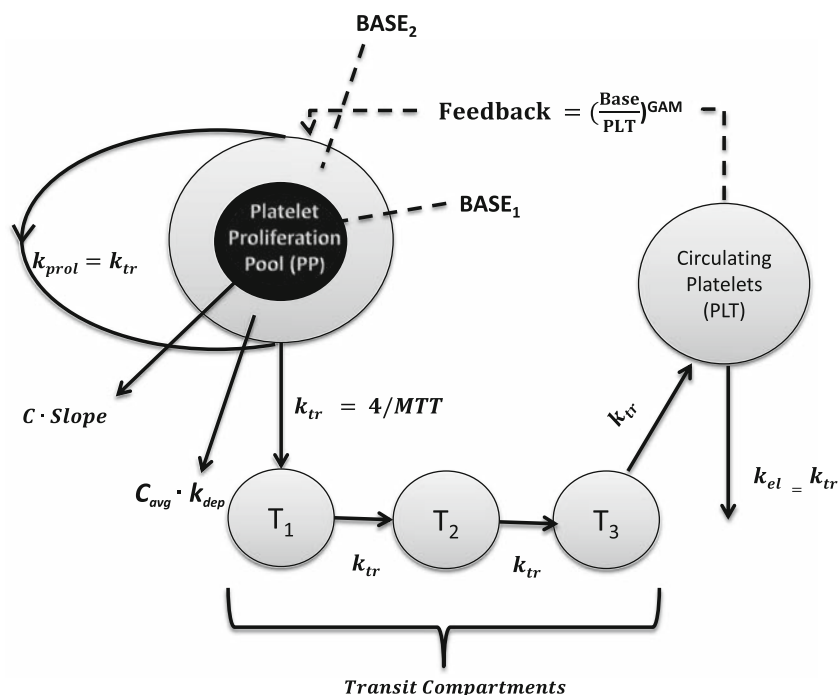
Many ADC induced clinical toxicities (*e.g.*, peripheral neuropathy, ocular toxicity, veno-occlusive disease *etc.*) are difficult to monitor on a continuous basis. Therefore, development of an exposure-toxicity relationship for these kind toxicities is very challenging. However, other ADC induced toxicities like the blood cell related toxicities (*e.g.*, neutropenia, thrombocytopenia *etc.*) and liver toxicity (measured using the biomarkers like aspartate transaminase and alanine transaminase) can be measured continuously as a part of clinical blood chemistry, and thus can be

employed for the development of clinical PK-PD (or more appropriately referred to as PK-TD) relationships.

Most of the PK-PD models developed for characterizing the exposure-toxicity relationships of ADCs in the clinic have been developed for thrombocytopenia (*i.e.*, abnormally low amount of platelets). And, these models have been developed based on a semi-mechanistic PK-PD model developed by Friberg *et al.* to characterize chemotherapy-induced myelosuppression (Fig. 6c) (35). Mugundu *et al.* have developed one such exposure-toxicity relationship for CMC-544, where they have correlated ADC or total drug (*i.e.*, conjugated + unconjugated calicheamicin) PK with the observed decrease in the platelet counts (44). They used the PK-PD model shown in Figure 6C, where the drug effect ( $E_{drug}$ ) was characterized in a nonlinear fashion using a sigmoidal  $E_{max}$  function. The exposure and toxicity data were obtained from five different phase- I/II studies conducted in follicular or diffuse large B-cell non-Hodgkin's lymphoma patients, who received CMC-544 at the doses ranging from 0.4 to 2.4 mg/m<sup>2</sup>. Using a sequential PK-PD analysis, the authors were able to characterize the PK and toxicity data reasonably well. Using the population PK-PD modeling the authors were also able to identify covariates that influenced the PK and platelet toxicity of CMC-544. They found that the baseline platelet count was a clinically significant covariate for CMC-544 induced thrombocytopenia, and suggested that it should be used for dose individualization. The integrated model of ADC/drug PK and platelet count also provided the authors a tool to identify optimal dosing schedules that would mitigate the incidence of thrombocytopenia in CMC-544 treated patients (44).

Bender *et al.* have also adapted the PK-PD model developed by Friberg *et al.* for characterizing the effect of T-DM1 on patients' platelet counts (Fig. 8) (38). Since the mAb alone (*i.e.*, trastuzumab), the drug alone (*i.e.*, DM1), and other DM1 containing ADCs have not demonstrated thrombocytopenia as the dose-limiting toxicity in the clinic, the authors chose to use conjugated mAb (*i.e.*, ADC) concentrations to correlate with the toxicity. A sequential PK-PD modeling approach was used, where the PK of TDM-1 was first characterized using a linear 2-compartment population PK model. The toxicity was characterized using the PD model developed by Friberg *et al.*, following two prominent modifications of the model. In order to account for the clinical observation where the platelet count nadirs were generally the lowest after the first T-DM1 dose, the model was modified to include separate efficacy parameters for the first dose and subsequent doses. The efficacy was characterized *via* the direct inhibitory effect of the plasma T-DM1 concentrations ( $C$ ) on the proliferation rate ( $k_{prol}$ ) of the proliferating platelet population ( $PP$ ), where *Slope1* and *Slope2* were used as the efficacy parameters for the first dose and subsequent doses. In order to account for another clinical observation where certain patients had platelet-time profiles that drifted downwards following multiple cycles

**Fig. 8** A PK-PD model developed to characterize T-DM1 induced thrombocytopenia in cancer patients (redrawn based on (38)).



of T-DM1 treatment, the model was modified to include two different populations of the proliferating platelets (PP): the baseline population-1 ( $BASE_1$ ) that was assumed to be nondepletable, and the baseline population-2 ( $BASE_2$ ) that was assumed to be depletable. The  $BASE_2$  population was assumed to be depleted via a first order processes ( $k_{dep}$ ), which was driven by  $C_{avg}$ , the average T-DM1 concentration observed over dosing intervals. Data from two different T-DM1 single-agent clinical studies were used for model development, and the data from a separate phase-II study were used for model evaluation. The PK-PD model was able to accurately capture the lowest platelet nadir after the 1st cycle, the downward drift in 46% patients' platelet-time profiles, and ~8% incidences of grade 3 or more thrombocytopenia in patients treated with 3.6 mg/kg of T-DM1 every 3 week (38). The model also predicted that the downward drifting of platelet-time profiles observed following T-DM1 treatment will be stabilized by the 18th treatment cycle, to platelet counts above grade 3 thrombocytopenia. Thus, the clinical PK-PD model developed for characterizing T-DM1 induced thrombocytopenia supported 3.6 mg/kg every 3 week as a well-tolerated dosing regimen for T-DM1, which is associated with minimal dose delays or reductions due to thrombocytopenia.

## SUMMARY

In this review we have presented the PK-PD models applicable to ADCs, and have emphasized their applications at different drug development stages. The importance of PK-PD

modeling and simulation in guiding the rationale discovery and development of ADCs is also highlighted. There is an array of PK-PD models, ranging from the systems models specifically developed for ADCs to the empirical models applicable to all chemotherapeutic agents, which one can employ for ADCs. The decision about which model to choose depends on the questions to be answered and the availability of time and resources. In order to realize the MBDD of ADCs, PK-PD modeling process should be started from the discovery stage itself, and the bioanalytical measurements should be committed with PK-PD modelers' perspective in mind (5). This will provide an opportunity to quantitatively integrate the experimental data generated at each-stage of development to support key go/no-go decisions. It is also important to bear in mind that our clinical experience with ADCs is limited, and in the future the PK-PD models are bound to improve. Additionally, our mechanistic understanding of ADC disposition, efficacy, and toxicity is also limited, and there is a need to conduct novel experiments, to help develop more mechanistic and reliable PK-PD models for ADCs.

## REFERENCES

1. Sassoon I, Blanc V. Antibody-drug conjugate (ADC) clinical pipeline: a review. *Methods Mol Biol.* 2013;1045:1–27.
2. Minich SS. Brentuximab vedotin: a new age in the treatment of Hodgkin lymphoma and anaplastic large cell lymphoma. *Ann Pharmacother.* 2012;46(3):377–83.

3. Gerber HP, Koehn FE, Abraham RT. The antibody-drug conjugate: an enabling modality for natural product-based cancer therapeutics. *Nat Prod Rep*. 2013;30(5):625–39.
4. Mullard A. Maturing antibody-drug conjugate pipeline hits 30. *Nat Rev Drug Discov*. 2013;12(5):329–32.
5. Shah DK, Barletta F, Betts A, Hansel S. Key bioanalytical measurements for antibody-drug conjugate development: PK/PD modelers' perspective. *Bioanalysis*. 2013;5(9):989–92.
6. Milligan PA, Brown MJ, Marchant B, Martin SW, van der Graaf PH, Benson N, *et al*. Model-based drug development: a rational approach to efficiently accelerate drug development. *Clin Pharmacol Ther*. 2013;93(6):502–14.
7. Shah DK, Haddish-Berhane N, Betts A. Bench to bedside translation of antibody drug conjugates using a multiscale mechanistic PK/PD model: a case study with brentuximab-vedotin. *J Pharmacokinet Pharmacodyn*. 2012;39(6):643–59.
8. Jackson D, Atkinson J, Guevara CI, Zhang C, Kery V, Moon SJ, *et al*. In vitro and in vivo evaluation of cysteine and site specific conjugated herceptin antibody-drug conjugates. *PLoS ONE*. 2014;9(1):e83865.
9. Okeley NM, Miyamoto JB, Zhang X, Sanderson RJ, Benjamin DR, Sievers EL, *et al*. Intracellular activation of SGN-35, a potent anti-CD30 antibody-drug conjugate. *Clin Cancer Res Off J Am Assoc Cancer Res*. 2010;16(3):888–97.
10. Haddish-Berhane N, Shah DK, Ma D, Leal M, Gerber HP, Sapra P, *et al*. On translation of antibody drug conjugates efficacy from mouse experimental tumors to the clinic: a PK/PD approach. *J Pharmacokinet Pharmacodyn*. 2013;40(5):557–71.
11. Hamed SS, Roth CM. Mathematical modeling to distinguish cell cycle arrest and cell killing in chemotherapeutic concentration response curves. *J Pharmacokinet Pharmacodyn*. 2011;38(3):385–403.
12. Muller PY, Milton MN. The determination and interpretation of the therapeutic index in drug development. *Nat Rev Drug Discov*. 2012;11(10):751–61.
13. Gorovits B, Alley SC, Bilic S, Booth B, Kaur S, Oldfield P, *et al*. Bioanalysis of antibody-drug conjugates: American Association of Pharmaceutical Scientists Antibody-Drug Conjugate Working Group position paper. *Bioanalysis*. 2013;5(9):997–1006.
14. Wagner-Rousset E, Janin-Bussat MC, Colas O, Excoffier M, Ayoub D, Haeuw JF, *et al*. Antibody-drug conjugate model fast characterization by LC-MS following IdeS proteolytic digestion. *mAbs*. 2014;6(1):273–85.
15. Bender B, Leipold DD, Xu K, Shen BQ, Tibbitts J, Friberg LE. A mechanistic pharmacokinetic model elucidating the disposition of trastuzumab emtansine (T-DM1), an antibody-drug conjugate (ADC) for treatment of metastatic breast cancer. *AAPS J*. 2014.
16. Hamblett KJ, Senter PD, Chace DF, Sun MM, Lenox J, Cerveny CG, *et al*. Effects of drug loading on the antitumor activity of a monoclonal antibody drug conjugate. *Clin Cancer Res Off J Am Assoc Cancer Res*. 2004;10(20):7063–70.
17. Panowski S, Bhakta S, Raab H, Polakis P, Junutula JR. Site-specific antibody drug conjugates for cancer therapy. *mAbs*. 2014;6(1):34–45.
18. Sukumaran S, Gadkar K, Zhang C, Bhakta S, Xu K, Raab H, *et al*. Mechanism-based pharmacokinetic/pharmacodynamics model for THIOMAB drug conjugates. Annual conference of American Association of Pharmaceutical Sciences (AAPS). Texas; 2013. Poster # T3237.
19. Shah DK, King LE, Han X, Wentland JA, Zhang Y, Lucas J, *et al*. A priori prediction of tumor payload concentrations: preclinical case study with an auristatin-based anti-5T4 antibody-drug conjugate. *AAPS J*. 2014;16(3):452–63.
20. Schmidt MM, Wittrup KD. A modeling analysis of the effects of molecular size and binding affinity on tumor targeting. *Mol Cancer Ther*. 2009;8(10):2861–71.
21. Thurber GM, Schmidt MM, Wittrup KD. Factors determining antibody distribution in tumors. *Trends Pharmacol Sci*. 2008;29(2):57–61.
22. Thurber GM, Zajic SC, Wittrup KD. Theoretic criteria for antibody penetration into solid tumors and micrometastases. *J Nucl Med Off Publ, Soc Nucl Med*. 2007;48(6):995–9.
23. Thurber GM, Weissleder R. A systems approach for tumor pharmacokinetics. *PLoS ONE*. 2011;6(9):e24696.
24. Shah DK, Balthasar JP. Physiologically based pharmacokinetic model for topotecan in mice. *J Pharmacokinet Pharmacodyn*. 2011;38(1):121–42.
25. Shah DK, Betts AM. Towards a platform PBPK model to characterize the plasma and tissue disposition of monoclonal antibodies in preclinical species and human. *J Pharmacokinet Pharmacodyn*. 2012;39(1):67–86.
26. Shah DK, Balthasar JP. Predicting the effects of 8C2, a monoclonal anti-topotecan antibody, on plasma and tissue disposition of topotecan. *J Pharmacokinet Pharmacodyn*. 2014;41(1):55–69.
27. Shah DK, Balthasar JP. PK/TD modeling for prediction of the effects of 8C2, an anti-topotecan mAb, on topotecan-induced toxicity in mice. *Int J Pharm*. 2014;465(1–2):228–38.
28. Garg A, Balthasar JP. Physiologically-based pharmacokinetic (PBPK) model to predict IgG tissue kinetics in wild-type and FcRn-knockout mice. *J Pharmacokinet Pharmacodyn*. 2007;34(5):687–709.
29. Shah DK, Betts AM. Antibody biodistribution coefficients: inferring tissue concentrations of monoclonal antibodies based on the plasma concentrations in several preclinical species and human. *mAbs*. 2013;5(2):297–305.
30. Zhao B, Zheng S, Alley SC. Physiologically-based pharmacokinetic modeling of an anti-CD70 auristatin antibody-drug conjugate in tumor-bearing mice. American Conference on Pharmacometrics (ACoP). San Diego; 2011.
31. Chen Y, Samineni D, Mukadam S, Wong H, Shen BQ, Lu D, *et al*. Physiologically based pharmacokinetic modeling as a tool to predict drug interactions for antibody-drug conjugates. *Clin Pharmacokinet*. 2014.
32. Simeoni M, Magni P, Cammia C, De Nicolao G, Croci V, Pesenti E, *et al*. Predictive pharmacokinetic-pharmacodynamic modeling of tumor growth kinetics in xenograft models after administration of anticancer agents. *Cancer Res*. 2004;64(3):1094–101.
33. Lobo ED, Balthasar JP. Pharmacodynamic modeling of chemotherapeutic effects: application of a transit compartment model to characterize methotrexate effects in vitro. *AAPS Pharmsci*. 2002;4(4):E42.
34. Jumbe NL, Xin Y, Leipold DD, Crocker L, Dugger D, Mai E, *et al*. Modeling the efficacy of trastuzumab-DM1, an antibody drug conjugate, in mice. *J Pharmacokinet Pharmacodyn*. 2010;37(3):221–42.
35. Friberg LE, Henningsson A, Maas H, Nguyen L, Karlsson MO. Model of chemotherapy-induced myelosuppression with parameter consistency across drugs. *J Clin Oncol Off J Am Soc Clin Oncol*. 2002;20(24):4713–21.
36. Tatipalli M, Derendorf H. Semi-physiological population PK/PD model of ADC neutropenia. M.S. Thesis. Pharmaceutical Sciences. Gainesville: University of Florida; 2012.
37. Gupta M, Lorusso PM, Wang B, Yi JH, Burris 3rd HA, Beeram M, *et al*. Clinical implications of pathophysiological and demographic covariates on the population pharmacokinetics of trastuzumab emtansine, a HER2-targeted antibody-drug conjugate, in patients with HER2-positive metastatic breast cancer. *J Clin Pharmacol*. 2012;52(5):691–703.
38. Bender BC, Schaedeli-Stark F, Koch R, Joshi A, Chu YW, Rugo H, *et al*. A population pharmacokinetic/pharmacodynamic model of thrombocytopenia characterizing the effect of trastuzumab emtansine (T-DM1) on platelet counts in patients with HER2-positive metastatic breast cancer. *Cancer Chemother Pharmacol*. 2012;70(4):591–601.
39. Lu D, Joshi A, Wang B, Olsen S, Yi JH, Krop IE, *et al*. An integrated multiple-analyte pharmacokinetic model to characterize trastuzumab emtansine (T-DM1) clearance pathways and to evaluate reduced

- pharmacokinetic sampling in patients with HER2-positive metastatic breast cancer. *Clin Pharmacokinet*. 2013;52(8):657–72.
40. Chudasama VL, Schaedeli Stark F, Harrold JM, Tibbitts J, Girish SR, Gupta M, *et al*. Semi-mechanistic population pharmacokinetic model of multivalent trastuzumab emtansine in patients with metastatic breast cancer. *Clin Pharmacol Ther*. 2012;92(4):520–7.
41. Mager DE, Jusko WJ. General pharmacokinetic model for drugs exhibiting target-mediated drug disposition. *J Pharmacokinet Pharmacodyn*. 2001;28(6):507–32.
42. Gibiansky L, Gibiansky E. Target-mediated drug disposition model and its approximations for antibody-drug conjugates. *J Pharmacokinet Pharmacodyn*. 2014;41(1):35–47.
43. Luu K, Vandendries E, Volkert A, Ogura M, Goy G, Boni J. Antitumor response to inotuzumab ozogamicin (INO) in patients with refractory or relapsed indolent B-cell non-Hodgkin's lymphomas (NHL): pharmacokinetic-pharmacodynamic (PK-PD) modeling and interim results from a phase II study AACR 103rd Annual Meeting Chicago; 2012. Poster # 7114.
44. Mugundu G, Vandendries E, Boni J. Use of pharmacokinetic-pharmacodynamic modeling to characterize platelet response following inotuzumab ozogamicin treatment in patients with follicular or diffuse large B-cell non-Hodgkin's lymphoma AACR 103rd Annual Meeting Chicago; 2012. Poster # 3776.